

Neck configuration of Cm and Cf nuclei in the fission state within relativistic mean field formalism

M. Bhuyan^{1,*}, B. V. Carlson^{1,†}, S. K. Patra^{3,‡} and Raj K. Gupta^{4,§}

¹*Instituto Tecnológico de Aeronáutica, 12.228-900 São José dos Campos, São Paulo, Brazil*

³*Institute of Physics, Sachivalaya Marg, Sainik School, Bhubaneswar 751005, India and*

⁴*Department of Physics, Panjab University, Chandigarh, Punjab 160014, India*

(Dated: March 16, 2022)

A correlation is established between the neutron multiplicity and the neutrons number in the fission state of Curium and Californium isotopes within a microscopic study using relativistic mean field formalism. The study includes the isotopes of Cm and Cf nuclei near the valley of stability, and hence is likely to play an important role in the artificial synthesis of superheavy nuclei. The static fission path, the neutron–proton asymmetry, the evolution of the neck and their composition in terms of nucleon numbers are also estimated. We find a maximum ratio for average neutron to proton density, which is about 1.6 in the breakdown of the liquid–drop picture for ²⁴⁸Cm and ²⁵²Cf. A strong dependence of the neutron–proton asymmetry on the neutron multiplicity in an isotopic chain is also observed.

PACS numbers: 21.65.Mn, 26.60.Kp, 21.65.Cd

I. INTRODUCTION

The first interpretation of nuclear fission was made about eight decades ago, though many features of this process are still in the rudimentary stage. The discovery of nuclear fission [1] was recognized as an evolution of the nuclear shape from a single compound nucleus split into two receding fragments [2, 3]. This conceptual framework within the macroscopic-microscopic approach to the calculation of nuclear binding energies, provides a powerful theoretical tool for studies of low-energy fission dynamics. Further analysis from the microscopic theories to exploration of its dynamics are also prime objective at present in nuclear physics. In order to explain the fission properties of superheavy nuclei, it is essential to measure the shape (i.e. height and width) of the barriers and shape degrees of freedom [3–8]. In early days, the fission shapes were investigated by minimizing the sum of the Coulomb and surface energies using a development of the radius in the Liquid Drop Model (LDM). Recently, fusion studies have shown that the effects of the nuclear forces in the neck region (i.e. the gap between two fragments) of the deformed valley are indeed needed for optimizing the proximity energy of the fission process. The goal is more or less reached by following the studies from macroscopic-microscopic (mic-mac) model [9–14], the extended Thomas-Fermi with Strutinsky integral (ETFSI) method [15, 16], non-relativistic Skyrme-Hartree-Fock [17–22], Gogny force [23–26], and relativistic mean field models [27–35].

The use of the adiabatic approximation in fission process is an interpretation of the potential energy surface

(PES), an analogue of the classical phase space of Lagrangian and Hamiltonian mechanics. The fission point of a nucleus can be determined from the total nuclear potential energy as a function of the shape coordinates relative to the ground state of the most favorable saddle point where the configuration evolves from a single nucleus into two separated fragments. The current way to deal with the splitting fragments depends on the most relevant collective variables of the nuclear shape, such as elongation, reflection asymmetry and neck structure that can be described by the multi-polarity deformations [24, 33, 34, 36]. Furthermore a critical feature of the fission process is the multiplicity of neutron and/or small $N=Z$ nuclei from the two fragments at the post scission point after they are accelerated by the mutual Coulomb repulsion [29, 37–39]. In this process, the neck is believed to be neutron rich and favorable for neutron emission than that of the proton and/or α -particle emission. At present, it is not possible to ascertain the true composition of the neck experimentally, which has the potential to reveal many important aspects of the fission dynamics.

The PES spanned by the relevant degrees-of-freedom of a fissile nucleus can be used to reveal a static fission path, fission lifetime, mass of the fragments and also many features of fission dynamics [26, 29, 33–36, 40–42]. To generate the neck structure of actinide nuclei and to determine the constituents of the neck (i.e. the average neutron-proton asymmetry and the neutron multiplicity) quantitatively, can be used to benchmark the predictive power of theoretical models [26, 29, 30, 33, 34, 37, 43, 44]. Such a study would be a step forward in the understanding of the fission dynamics of actinide nuclei [29, 33, 35] and the synthesis process in the experimental laboratories available at present or/and under construction around the world [45–53]. Further the composition of the neck in the fission state of actinide nuclei may involve information regarding the formation of the elements in the rapid neutron capture process (i.e. r -process) of nuclear syn-

* Email: bhuyan@ita.br

† Email: brettvc@gmail.com

‡ Email: patra@iopb.res.in

§ Email: rajkgupta.chd@gmail.com

thesis in stellar evolution [54–56]. In the present study we examine the properties of the fission state of actinides using the axially deformed relativistic mean field (RMF) model.

This paper is organized as follows: In Sec. II we outline our scheme of the calculations using the relativistic mean field approach. The calculations and results are given in Sec. III. Finally, a summary and brief conclusion are given in Sec. IV.

II. THEORETICAL FORMALISMS

The microscopic self-consistent mean field calculation is one of the standard tools to investigate the properties of infinite nuclear matter and nuclear structure phenomena [17, 18, 21, 22, 26, 33–35, 40–42, 57–59]. The relativistic mean field (RMF) approach is one of the most popular and widely used formalisms among them. It starts with a basic Lagrangian that describes nucleons as Dirac spinors interacting through different meson fields. The relativistic mean field Lagrangian density, which has several modifications to account for various limitations of Walecka Lagrangian [57, 58] for a nucleon-meson many body system [57–77], is

$$\begin{aligned} \mathcal{L} = & \bar{\psi}\{i\gamma^\mu\partial_\mu - M\}\psi + \frac{1}{2}\partial^\mu\sigma\partial_\mu\sigma \\ & - \frac{1}{2}m_\sigma^2\sigma^2 - \frac{1}{3}g_2\sigma^3 - \frac{1}{4}g_3\sigma^4 - g_s\bar{\psi}\psi\sigma \\ & - \frac{1}{4}\Omega^{\mu\nu}\Omega_{\mu\nu} + \frac{1}{2}m_\omega^2\omega^\mu\omega_\mu - g_\omega\bar{\psi}\gamma^\mu\psi\omega_\mu \\ & - \frac{1}{4}\vec{B}^{\mu\nu}\cdot\vec{B}_{\mu\nu} + \frac{1}{2}m_\rho^2\vec{\rho}^\mu\cdot\vec{\rho}_\mu - g_\rho\bar{\psi}\gamma^\mu\vec{\tau}\psi\cdot\vec{\rho}^\mu \\ & - \frac{1}{4}F^{\mu\nu}F_{\mu\nu} - e\bar{\psi}\gamma^\mu\frac{(1-\tau_3)}{2}\psi A_\mu. \end{aligned} \quad (1)$$

The ψ is the Dirac spinor for the nucleon whose third component of isospin is denoted by τ_3 . Here g_σ , g_ω , g_ρ and $\frac{e^2}{4\pi}$ are the coupling constants for the σ -, ω -, ρ -meson and photon, respectively. The constant g_2 and g_3 are for the self-interacting non-linear σ -meson field. The masses of the σ -, ω -, ρ -mesons and nucleons are m_σ , m_ω , m_ρ , and M respectively. The quantity A_μ stands for the electromagnetic field. The vector field tensors for the ω^μ , $\vec{\rho}_\mu$ and photon are given by,

$$F^{\mu\nu} = \partial_\mu A_\nu - \partial_\nu A_\mu \quad (2)$$

$$\Omega_{\mu\nu} = \partial_\mu\omega_\nu - \partial_\nu\omega_\mu \quad (3)$$

and

$$\vec{B}^{\mu\nu} = \partial_\mu\vec{\rho}_\nu - \partial_\nu\vec{\rho}_\mu, \quad (4)$$

respectively. From the above Lagrangian, we obtain the field equations for the nucleons and mesons. These equations are solved by expanding the upper and lower components of the Dirac spinors and the boson fields in an axially deformed harmonic oscillator basis, with an initial deformation β_0 . The set of coupled equations are

solved numerically by a self-consistent iteration method [44, 78–80]. The center-of-mass motion energy correction is estimated by the harmonic oscillator formula $E_{c.m.} = \frac{3}{4}(41A^{-1/3})$. The quadrupole deformation parameter β_2 is evaluated from the resulting proton and neutron quadrupole moments, as

$$Q = Q_n + Q_p = \sqrt{\frac{16\pi}{5}}\left(\frac{3}{4\pi}AR^2\beta_2\right). \quad (5)$$

The root mean square (rms) matter radius is defined as

$$\langle r_m^2 \rangle = \frac{1}{A} \int \rho(r_\perp, z) r^2 d\tau, \quad (6)$$

where A is the mass number, and $\rho(r_\perp, z)$ is the axially deformed density. We obtain the potentials, nucleon densities, single-particle energy levels, nuclear radii, quadrupole deformations and the binding energies for a given nucleus. Converged ground state along with various constraint solutions can be obtained at different deformations including fission state of a nucleus (see the potential energy surface).

To deal with the nuclear bulk properties of open-shell nuclei, one has to consider the pairing correlations [81]. There are various methods such as the BCS approach, the Bogoliubov transformation and the particle number conserving methods that have been developed to treat the pairing effects in the study of nuclear properties including fission barriers [82–84]. The Bogoliubov transformation is widely used method to take pairing correlation into account for the drip-line region [64, 65, 70, 85]. In the case of nuclei not too far from the β -stability line, the constant gap BCS pairing approach provides a reasonably good description of pairing [86]. The present analysis is based on the superheavy mass nuclei around the β -stability line, hence the relativistic mean field results with BCS treatment should be applicable. Further, to avoid difficulties in the calculations, we have employed the constant gap BCS approach to deal with the present mass region [34, 61, 87–89].

III. CALCULATIONS AND RESULTS

In the relativistic mean field model, we performed the self-consistent calculation for maximum boson major shell number $N_B = 20$ and varying maximum nucleon major shell number N_F from 14 to 24 to verify the convergence of the solutions by taking different inputs of initial deformation β_0 for the ground state [61, 69, 76, 77]. From the results obtained, we found that the relative variations of the ground state solutions are $\leq 0.004\%$ for the binding energy and 0.002% for the nuclear radius. In the case of fission state solutions, the binding energy and nuclear radius varies $\leq 0.01\%$ and 0.006% , respectively over the range of major shell fermion number N_F from 16 to 28 for $N_B = 24$. Hence, we fixed that the number of major shells for fermions and bosons at $N_F = N_B = 20$ and $N_F = N_B = 24$ for the ground

TABLE I. The RMF (NL3*) results for the binding energy (BE), root-mean-square charge radii r_{ch} and the quadrupole deformation parameter β_2 for $^{242,244,246,248}\text{Cm}$ and $^{248,250,252,254}\text{Cf}$ nuclei. The ground state, the constraint minima for first, second and fission states are given in the 1st, 2nd, 3rd, and 4th row for each nucleus. The Finite-Range-Droplet-Model [90, 91], Hartree-Fock + BCS [92] and the experimental data [93–95] for the ground state configurations are given for comparison, wherever available. The energies are in *MeV* and radii in *fm*.

Nucleus	Binding Energy			Charge Radius			Quadrupole Deformation			
	RMF	Expt. [93]	FRDM [90]	RMF	Expt. [94]	HFBCS [92]	RMF	Expt. [95]	FRDM [91]	HFBCS [92]
^{242}Cm	1823.92	1823.3	1823.05	5.933	5.8285	5.90	0.287	—	0.224	0.25
	1822.82			6.560			0.969			
	1822.51			8.143			2.313			
	1693.64			11.089			5.036			
^{244}Cm	1836.24	1835.8	1835.79	5.946	5.8429	5.91	0.293	0.2972(17)	0.234	0.25
	1835.12			6.554			0.959			
	1821.33			8.455			2.475			
	1704.21			11.086			5.010			
^{246}Cm	1847.34	1847.8	1847.86	5.947	5.8475	5.93	0.293	0.2983(19)	0.234	0.27
	1845.75			6.553			0.921			
	1833.16			8.449			2.464			
	1714.82			10.982			4.984			
^{248}Cm	1860.63	1859.2	1859.28	5.959	5.8562	5.94	0.290	0.2972(19)	0.235	0.28
	1859.31			6.556			0.916			
	1844.72			8.474			2.453			
	1724.72			10.965			4.957			
^{248}Cf	1861.11	1857.8	1857.82	5.990	—	5.95	0.288	—	0.235	0.25
	1859.83			6.624			0.969			
	1847.22			8.554			2.490			
	1726.41			11.115			4.973			
^{250}Cf	1872.90	1870.0	1870.29	6.001	—	5.96	0.285	0.299 (15)	0.245	0.28
	1871.81			6.641			0.967			
	1859.51			8.568			2.479			
	1736.83			11.076			4.945			
^{252}Cf	1883.82	1881.3	1881.32	6.011	—	5.97	0.278	—	0.236	0.25
	1882.64			6.681			1.081			
	1871.61			8.581			2.461			
	1710.73			10.972			4.884			
^{254}Cf	1893.25	1892.2	1891.69	6.022	—	5.97	0.272	—	0.226	0.24
	1891.96			6.987			1.083			
	1820.45			8.593			2.460			
	1820.73			10.843			4.838			

state and for the fission state of the considered mass region, respectively. The number of mesh points for Gauss-Hermite and Gauss-Lagurre integral are 20 and 24, respectively. We have used the recently developed NL3* force [69] for the present analysis, which is a version of

the NL3 force [77] refitted to improve the description for the properties of neutron- and/or proton-rich exotic and superheavy nuclei [30, 61, 69]. For a given nucleus, we find various constraint solutions including the fission state along with the ground state (see the potential curve

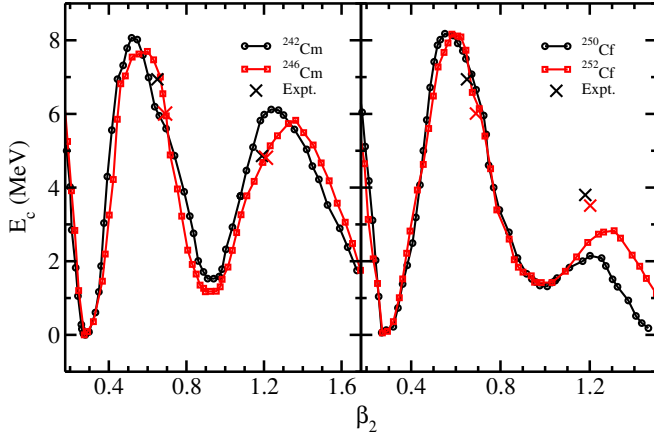


FIG. 1. (Color online) The RMF (NL3*) potential energy surfaces (PES) of $^{242,246}\text{Cm}$ and $^{248,252}\text{Cf}$ as a function of the quadrupole deformation parameter β_2 are displayed with the empirical values [96] for the first and second barrier heights. Note that the reflection symmetry is assumed in the present calculation. Heights are in MeV. See text for details.

Fig. 1). The calculated bulk properties such as binding energy (BE), root-mean-square (rms) charge radius, and quadrupole deformation β_2 for the ground state, first, second, third constraint and fission solutions are given in the first, second, third and fourth rows for a given nucleus, respectively. The results obtained from NL3* force listed together with the predictions from Finite-Range-Droplet-Model (FRDM) [90, 91], Hartree-Fock + BCS (HFBCS) [92] and the experimental data [93–95]. Since BE values are not available for HFBCS predictions, we have listed the rms charge radius r_{ch} , and the quadrupole deformation β_2 for comparisons. We find that the ground state binding energies, charge radii and β_2 values agree well with the available experimental data [93–95] and the theoretical predictions [90–92].

As discussed above, all the isotopes of Cm and Cf are shown to have several intrinsic minima, where each minimum corresponds to a quadrupole deformation. For example, the ground state (g.s.), first excited state, second excited state and the fission state deformation β_2 for ^{242}Cm are 0.287, 0.969, 2.313 and 5.036, respectively. Similarly, the values are 0.288, 0.969, 2.490, and 4.973, respectively for ^{248}Cf . All other isotopes and their deformations for various minima including the fission state are listed in Table I. The solution corresponding to the highly deformed (hyper-deformed) configuration of $\beta_2 \sim 2.4$ for all isotopes provide a beautiful picture of the pre-fission state. In other words, very smooth hyper-deformed solutions followed the fission configurations for all the considered isotopes in the present study. Further, the rms charge radius r_{ch} gradually increases with increase of quadrupole deformation for a given nucleus.

TABLE II. The RMF (NL3*) results for the first and second barrier heights of even-even isotopes of Cm and Cf nuclei are compared with the empirical values (Emp.) [96]. Note that the reflection symmetry is assumed. Heights are in MeV.

Nucleus	First barrier		Second barrier	
	RMF	Emp. [96]	RMF	Emp. [96]
^{242}Cm	7.92	6.65	5.76	5.10
^{244}Cm	7.75	6.18	5.17	5.00
^{246}Cm	7.13	6.00	5.00	4.80
^{248}Cm	6.84	5.80	4.93	4.80
^{248}Cf	8.13	—	3.33	—
^{250}Cf	8.06	5.60	2.83	3.80
^{252}Cf	7.98	5.30	2.53	3.50
^{254}Cf	7.56	—	1.79	—

A. Potential Energy Surface

The potential energy surface (PES) is calculated by using the relativistic mean field formalism in a constrained procedure [30, 33, 34, 61, 97–99], i.e., instead of minimizing the H_0 , we have minimized $H' = H_0 - \lambda Q_2$. Here, λ is a Lagrange multiplier and Q_2 , the quadrupole moment. The term H_0 is the Dirac mean field Hamiltonian for the RMF model (the notations are standard and its form can be seen in Refs.[34, 76]). In other words, we obtain the constrained solution from the minimization of $\sum_{ij} \frac{\langle \psi_i | H_0 - \lambda Q_2 | \psi_j \rangle}{\langle \psi_i | \psi_j \rangle}$ and calculate the constrained binding energy using H_0 . The free energy is obtained from the minimization of $\sum_{ij} \frac{\langle \psi_i | H_0 | \psi_j \rangle}{\langle \psi_i | \psi_j \rangle}$ and the converged energy solution does not depend on the initial guess value of the basis deformation β_0 as long as it is nearer to the minimum in PES. However, it converges to some other local minimum when β_0 is drastically different, and in this way we evaluate the different intrinsic isomeric states for a given nucleus. Note that the reflection symmetry is assumed for the calculation of the potential energy surface of the even–even isotopes of the Cm and Cf nuclei considered.

The potential energy surface for $^{242,246}\text{Cm}$ (left panel) and $^{250,252}\text{Cf}$ (right panel) nuclei are shown in Fig. 1 for a wide range of β_2 starting from the spherical to hyper-deformed prolate configuration. The cross (X) signs in both panels are represented by the empirical values [96] of the first and second barrier heights of the respective nucleus. Here, we found multi-minima structure from the PES for each isotopes. In Fig. 1, we have shown the PES's of $^{242,246}\text{Cm}$ and $^{250,252}\text{Cf}$ as a representative case. From the figure, one can notice that two identical major minima exist at $\beta_2 \approx 0.29$ and 0.95 for ^{242}Cm and ^{246}Cm nuclei (see left panel of Fig. 1). Similarly, the minima also appear in case of $^{250,252}\text{Cf}$ nuclei at $\beta_2 \approx 0.28$ and 0.95 , respectively. We found similar results for all the

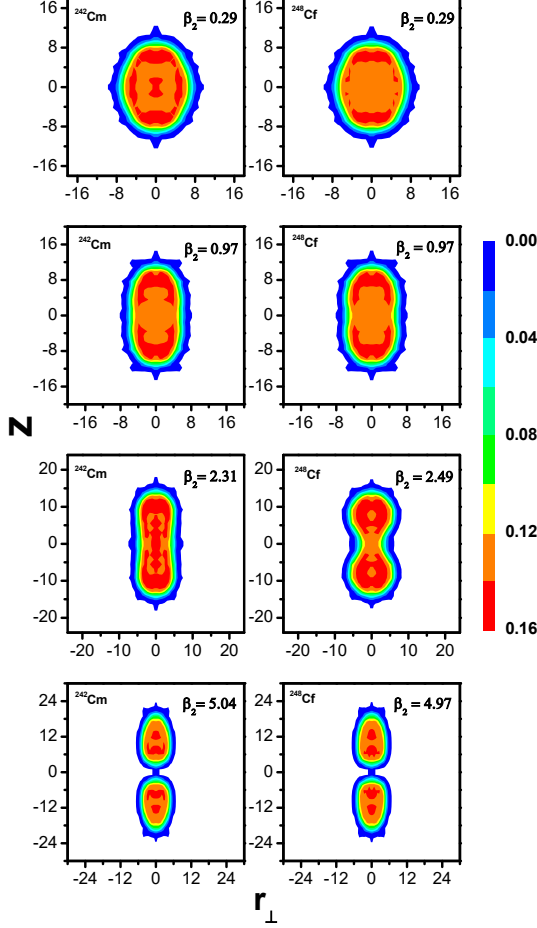


FIG. 2. (Color online) The evolution of static fission for the isotopes of ^{242}Cm (left) and ^{248}Cf (right) for different deformations β_2 corresponding to the possible minima obtained in the RMF formalism using the NL3* force parameter set. See text for details.

considered isotopes of Cm and Cf nuclei. The calculated first and second barrier heights for all the isotopes along with the empirical values [96] are listed in Table II. We notice that the quadrupole deformation parameters and the barrier heights obtained from our calculations reasonably agree with the empirical values [94, 96] of the isotopic chains of Cm and Cf nuclei, wherever available. For example, the obtained first and second barrier heights for ^{242}Cm are 7.92 and 5.76 MeV, respectively (see Table II). Similarly, the values are 8.06 and 2.83 MeV, respectively for ^{250}Cf (see Table II). The corresponding empirical values for the first and second barrier height for ^{242}Cm and ^{250}Cf are 6.65, 5.10 MeV and 5.60 and 3.80 MeV, respectively. Moreover, the calculated minima and/or the barriers in the PES shift a bit towards larger values of deformation β_2 in the isotopic chains.

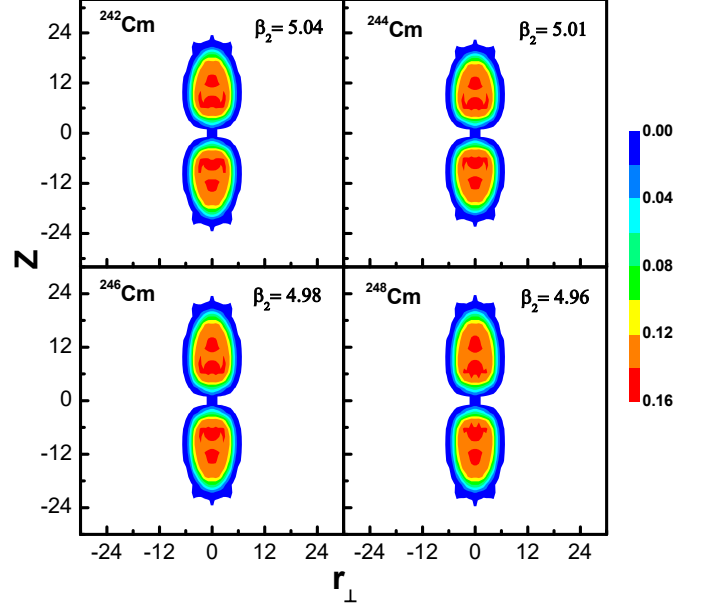


FIG. 3. (Color online) The RMF (NL3*) total (neutron + proton) matter density distribution for the fission states of the $^{242,244,246,248}\text{Cm}$ nuclei. See text for details.

B. Nuclear Density Distribution

The present calculations mainly explain the nuclear structure and sub-structure of the nucleus, which depend on the density distributions of the protons and neutrons for each corresponding state. The density distribution of the nucleus is influenced by the nuclear deformations, which play a prominent role in the fission study. Here, we calculate the densities for the positive quadrant of the plane parallel to the z -axis (i.e. the symmetry axis) and evaluated in the zr_\perp plane, where $x^2 + y^2 = r_\perp^2$. The space reflection symmetries about both the z and r_\perp axes are conserved in our formalism. The results for the density in the positive quadrant can be reflected in the other quadrants to get a complete picture of the nucleus in the zr_\perp plane. The unbroken space reflection symmetries of our numerical procedure eliminate the odd multipoles (octupole, etc.) shape degrees of freedom. In other words, there are limitations in explaining nuclei with an asymmetric partition of particles that will not be properly clustered in the asymptotic limit. Nevertheless, the present study demonstrates the applicability of the RMF for studying the nuclear fission phenomenon and provides the scope for understanding the nuclear structure of even-even nuclei. Further, this furnishes an indication of the nuclear structure and various sub-structure for various deformed states including the fission state.

The present calculations are performed in an axially deformed co-ordinate space. Consideration of the deformed coordinate space might solve some of these issues and will throw more light on the sub-structure of nuclei, which may be an interesting work for future.

In Fig. 2, we have presented typical examples for the matter density distributions of the ^{242}Cm and ^{248}Cf nuclei for all possible solutions, starting from the ground state up to their static fission configuration with a neck. The shape of the ^{242}Cm and ^{248}Cf nuclei follow the deformed ground state solution around $\beta_2 \approx 0.29$, and the super-deformed and hyper-deformed prolate solutions obtained around $\beta_2 \approx 0.97$ and 2.35 , respectively. Further, a well-defined dumbbell shape of the neck configuration is reproduced in the RMF study as a solution of the microscopic nuclear many-body Hamiltonian around $\beta_2 \approx 4.50$, in agreement with the age-old classical liquid drop picture of the fission process. The physical characteristics of the neck-structures for the isotopic chain of Cm and Cf systems emerging from this study will be discussed later. From Fig. 2, the internal configurations for ^{242}Cm and ^{248}Cf nuclei are quite evident and similar structures can be found for all the considered isotopes of Cm and Cf. The color code, starts from deep red with maximum density distribution to blue bearing the minimum density. One can analyze the distribution of nucleons inside the various isotopes at various shapes (in black and white figures, the color code is read as deep black with maximum density to light gray as minimum density distribution). The minimum density for the oblate-state starts from 0.001 fm^{-3} and goes up to a maximum of 0.16 fm^{-3} for all the shapes (see Fig. 2). One notices that the central density ($\rho \approx 0.16 \text{ fm}^{-3}$) becomes elongated with respect to deformation instead of changing in magnitudes (see the Table I and Fig. 2). Here, we also find the neck structures (i.e. the elongated shape with clear-cut neck before scission) similar to those of the microscopic study using the constrained method with Gogny interaction [100] and the Skyrme-Hartree-Fock [101]. In other words, the fissioning systems energetically favor splitting into two separate fragments by developing an elongated shape with a neck.

Since our objective has been to critically study the neck configurations, we have presented the matter density distributions for the fission states of our calculations for the four isotopes of Cm and Cf in Figs. 3 and 4, respectively. The binding energies, rms charge radii and quadrupole deformations of the neck configuration for $^{242,244,246,248}\text{Cm}$ and $^{248,250,252,254}\text{Cf}$ can be seen in Table I. As can be seen in Fig. 1, the neck configurations lie $\approx 15 \text{ MeV}$ below the respective ground states in conformity with the expectation and in agreement with our general notion of fission dynamics. Further, the rms charge radii for the neck configurations are nearly twice those of ground state, around 12 fm as expected. From the Figs. 3 and 4, it is clear that all the isotopes undergo symmetric fission, which is the limitation of the present model. Here, we see how far the neck structure for these isotopes conform to reality from the calculated values of the first

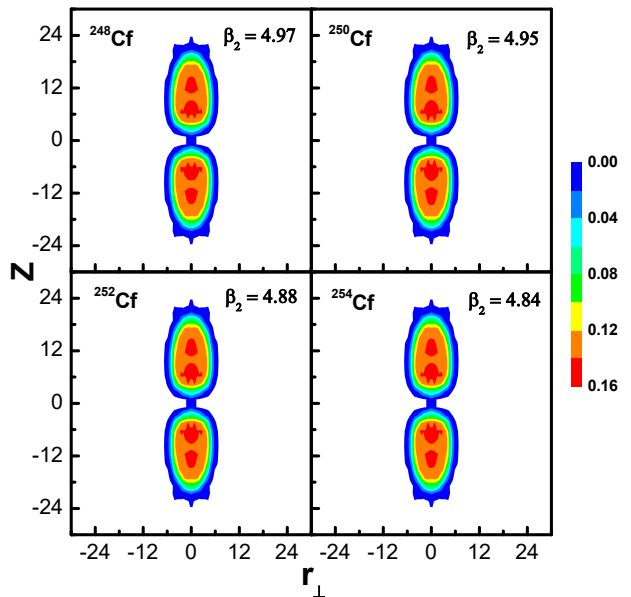


FIG. 4. (Color online) The RMF (NL3*) total (neutron + proton) matter density distribution for the fission states of the $^{248,250,252,254}\text{Cf}$ nuclei. See text for details.

and second barrier height, which reasonably agree with the empirical values (see Fig. 1 and Table II).

C. The Neck Characteristics

The calculated yields of the total number of neutrons N^{nk} and protons Z^{nk} contained in the neck are obtained by integrating the corresponding densities over the physical dimension of the neck. The number of nucleons for the neck regions can be calculated by,

$$N^{nk} = \int \int \rho_n^{nk}(r_\perp, z) d\tau, \quad (7)$$

and

$$Z^{nk} = \int \int \rho_p^{nk}(r_\perp, z) d\tau, \quad (8)$$

where ρ_n^{nk} and ρ_p^{nk} are the calculated RMF neutron and proton density distributions of the nucleus in the neck configuration, respectively. We also present the mean neutron and proton densities of the neck as,

$$\bar{\rho}_{n,p}^{nk} = \frac{\int \rho_{n,p}^{nk} d\tau}{\int d\tau}. \quad (9)$$

From Eq. 9, we estimate the average neutron $\bar{\rho}_n^{nk}$ and proton $\bar{\rho}_p^{nk}$ density and their ratio $\bar{\rho}_n^{nk}/\bar{\rho}_p^{nk}$ for the neck

TABLE III. The RMF(NL3*) characteristics of neck configurations such as the quadrupole deformation (β_2), charge radius r_{ch}^{nk} of the fission state, average neutron ($\bar{\rho}_n^{nk}$) and proton density ($\bar{\rho}_p^{nk}$) and their ratio ($\frac{\bar{\rho}_n^{nk}}{\bar{\rho}_p^{nk}}$) in the neck region, dimension of the neck, length of the neck (L^{nk}), the number of neutron (N^{nk}) and proton (Z^{nk}) of the neck for $^{242,244,246,248}\text{Cm}$ and $^{248,250,252,254}\text{Cf}$ are presented. See text for details.

Nucleus	β_2	r_{ch}^{nk}	$\bar{\rho}_n^{nk}$	$\bar{\rho}_p^{nk}$	$\frac{\bar{\rho}_n^{nk}}{\bar{\rho}_p^{nk}}$	Range ($r_1, r_2; z_1, z_2$)	L^{nk}	N^{nk}	Z^{nk}	$\frac{Z^{nk}}{N^{nk}}$	Nucleus ^{nk}
^{242}Cm	5.036	11.089	0.032	0.035	0.91	$\pm 2.28; \pm 1.25$	4.56	2.01	2.01	1.00	^2He
^{244}Cm	5.010	11.086	0.041	0.034	1.21	$\pm 2.28; \pm 1.25$	4.56	2.09	2.05	1.02	^2He
^{246}Cm	4.984	10.982	0.047	0.033	1.42	$\pm 2.28; \pm 1.25$	4.56	2.02	2.01	1.01	^4He
^{248}Cm	4.957	10.965	0.052	0.033	1.57	$\pm 2.28; \pm 1.25$	4.56	2.06	2.01	1.02	^4He
^{248}Cf	4.973	11.115	0.034	0.037	0.92	$\pm 2.27; \pm 1.26$	4.52	1.01	0.94	1.07	^4H
^{250}Cf	4.945	11.076	0.046	0.036	1.28	$\pm 2.27; \pm 1.26$	4.52	1.05	0.98	1.07	^4H
^{252}Cf	4.884	10.972	0.051	0.035	1.46	$\pm 2.27; \pm 1.26$	4.52	2.08	2.01	1.03	^4He
^{254}Cf	4.838	10.843	0.055	0.034	1.62	$\pm 2.27; \pm 1.26$	4.52	2.09	2.01	1.04	^4He

region. The estimates for the neutron and/or proton constituents and their asymmetry are listed in Table III for the $^{242,244,246,248}\text{Cm}$ and $^{242,244,246,248}\text{Cf}$ nuclei. As expected, the $\bar{\rho}_n^{nk}$ and $\bar{\rho}_p^{nk}$ for both the elements remain similar for all their isotopes being around 0.035 fm^{-3} (see Table III). The $\bar{\rho}_n^{nk}$ for the isotopic chains of Cm and Cf nuclei, gradually increase with the the neutron number. Furthermore, the neutron to proton density ratio $\bar{\rho}_n^{nk}/\bar{\rho}_p^{nk}$ increases gradually with respect to neutron number, as expected. In the isotopic chain of the Cm nuclei, the ratio has increased from 0.91 for ^{242}Cm to 1.57 for ^{248}Cm . The corresponding values are 0.92 for ^{248}Cf to 1.62 for ^{254}Cf (see Table III).

We have estimated the length of the neck in the fission state, which is quite important for determining the neck constituents. The length of the neck L^{nk} is the distance between the two facing connect surfaces. The width of the neck is not that important for the estimation of the constituents, using Eqs. 7 & 8, because it only averages out the sum of the matter densities within L_n . The length of the neck L_n and its constituents are listed in the Table III. From the Table III, one can find the charge radii of the neck configuration for all the isotopes, which are about 12 fm with a well-defined neck and fairly extended mass distribution evident in all cases. It is indeed interesting that heavy and superheavy nuclei acquire such an extended dumbbell configuration, supported by the nucleon-nucleon force [39, 102]. As we move from ^{242}Cm to ^{248}Cm , the number of neck neutron and neck proton numbers remain unchanged. A similar trend is seen for the Cf isotopes. It may be noticed that the magnitude of the ratio N^{nk}/Z^{nk} is some what different from that of the average neutron-to-proton neck densities $\bar{\rho}_n^{nk}/\bar{\rho}_p^{nk}$ (found in Table III). It shows that the effective volume distributions of neutrons and protons are different in the neck region. The ratio of neutron-to-proton number in the neck region found in our present

calculation is about 1.02 for all the isotopes of Cm and Cf nuclei. Hence, the neck can be considered as a quasi-bound transient state of any $N = Z$ nucleus with the neck nucleus correlated with those transient state being ^4He for all isotopes of Cm nuclei. In the case of Cf, the effective nucleus is np for $^{248,250}\text{Cf}$ and ^4He for $^{252,254}\text{Cf}$.

IV. SUMMARY AND CONCLUSIONS

In the present study, we have investigated the mechanism of fission decay and the shape of the nucleus by following the static fission path to the configuration before the breakup. The well established microscopic many-body nuclear Hamiltonian, i.e., the RMF theory is employed for estimating the classical liquid-drop picture of the fission state. The actinide isotopes of Cm and Cf nuclei near the valley of stability have been studied with the objective of relevance in stellar evolution. We found a deformed prolate configuration for the ground state of the isotopic chain for Cm and Cf nuclei. Furthermore, a highly deformed configuration with a neck is found by using a very large basis consisting of as many as 24 oscillator shells, while for the ground state 20 shells are adequate. This study has revealed the anatomy of the neck in the fission state, such as the average neutron-proton asymmetry, the length and their composition. We found that the average neutron-proton ratio of the neck region progressively increases with the neutron number in the isotopic chains of Cm and Cf nuclei. The neutron-to-proton number ratio found in our calculation is 1.02, which may correlate with the quasi-bound and/or a resonance state of a light $N = Z$ nucleus and /or α -particle. The necks found in the calculation at the above exotic nuclei suggest a point where along with the two heavy fragments, an α -particle might be emitted at scission for the considered isotopes of Cm and Cf nuclei, except

$^{248,250}\text{Cf}$. In case of $^{248,250}\text{Cf}$, we found the neck constituents are to be np with the two symmetry fragments in the fission. Due to the symmetry in the neutron-proton ratio of the neck, this cannot be strained into the two fragments at scission, but itself breaks down by emitting these nucleons which might be observed from the scission mass-yield studies. This would have strong implication in the energy generation of r -process nucleosynthesis in stellar evolution.

ACKNOWLEDGMENTS

This work has been supported by the FAPESP Project Nos. (2014/26195-5 & 2017/05660-0), INCT-FNA Project No. 464898/2014-5, and by the CNPq - Brasil. The authors thank Shan-Gui Zhou for his many-fold discussions through out the work.

-
- [1] O. Hahn and F. Strassmann, *Die Naturwissenschaften* **27**, 11 (1939).
 - [2] L. Meitner and O. R. Fritsch, *Nature* **143**, 239 (1939).
 - [3] N. Bohr and J. A. Wheeler, *Phys. Rev.* **56**, 426 (1939).
 - [4] S. Hofmann and G. Münzenberg, *Rev. Mod. Phys.* **72**, 733 (2000).
 - [5] Y. Oganessian, *J. Phys. G: Nucl. Phys.* **34**, R165 (2007).
 - [6] Y. T. Oganessian *et al.*, *Phys. Rev. Lett.* **104**, 142502 (2010).
 - [7] P. Möller, A. J. Sierk, T. Ichikawa, A. Iwamoto, R. Bengtsson, H. Uhrenholt, and S. Aberg, *Phys. Rev. C* **79**, 064304 (2009).
 - [8] Z.-H. Liu and J.-D. Bao, *Phys. Rev. C* **84**, 031602 (2011).
 - [9] P. Möller, D. G. Madland, A. J. Sierk, and A. Iwamoto, *Nature* **409**, 785 (2001).
 - [10] A. Dobrowolski, K. Pomorski, and J. Bartel, *Phys. Rev. C* **75**, 024613 (2007).
 - [11] F. A. Ivanyuk and K. Pomorski, *Phys. Rev. C* **79**, 054327 (2009).
 - [12] M. Kowal, P. Jachimowicz, and A. Sobiczewski, *Phys. Rev. C* **82**, 014303 (2010).
 - [13] G. Royer, M. Jaffre, and D. Moreau, *Phys. Rev. C* **86**, 044326 (2012).
 - [14] C.-L. Zhong, and T.-S. Fan, *Commun. Theor. Phys.* **62**, 405 (2014).
 - [15] A. Mamdouh, J. M. Pearson, M. Rayet, and F. Tondeur, *Nucl. Phys. A* **644**, 389 (1998).
 - [16] L. Ghys, A. N. Andreyev, S. Antalic, M. Huyse, and P. Van Duppen, *Phys. Rev. C* **91**, 044314 (2015).
 - [17] T. Burvenich, M. Bender, J. A. Maruhn, and P.-G. Reinhard, *Phys. Rev. C* **69**, 014307 (2004).
 - [18] M. Samyn, S. Goriely, and J. M. Pearson, *Phys. Rev. C* **75**, 064312 (2007).
 - [19] F. Minato, S. Chiba, and K. Hagino, *Nucl. Phys. A* **831**, 150 (2009).
 - [20] J. C. Pei, W. Nazarewicz, J. A. Sheikh, and A. K. Kerman, *Phys. Rev. Lett.* **102**,
 - [21] P. Goddard, P. Stevenson, and A. Rios, *Phys. Rev. C* **92**, 054610 (2015).
 - [22] Yi Zhu, and J. C. Pei, *Phys. Rev. C* **94**, 024329 (2016).
 - [23] J. L. Egido, and L. M. Robledo, *Phys. Rev. Lett.* **85**, 1198 (2000).
 - [24] M. Warda, K. Pomorski, J. L. Egido, and L M Robledo, *J. Phys. G: Nucl. Part. Phys.* **31**, S1555 (2005).
 - [25] M. Warda and J. L. Egido, *Phys. Rev. C* **86**, 014322 (2012).
 - [26] G. F. Bertsch, *Int. J. Mod. Phys. E*, **26**, 1740001 (2017)
 - [27] M. Bender, P.-H. Heenen, and P.-G. Reinhard, *Rev. Mod. Phys.* **75**, 121 (2003).
 - [28] H.-F. Lü, L.-S. Geng, and J. Meng, *Chin. Phys. Lett.* **23**, 2940 (2006).
 - [29] S. K. Patra, R. K. Choudhury, and L. Satpathy, *J. Phys. G: Nucl. Part. Phys.* **37**, 085103 (2010).
 - [30] M. Bhuyan, S. K. Patra, P. Arumugam, and Raj K. Gupta, *Int. J. Mod. Phys. E* **20**, 1227 (2011).
 - [31] B.-N. Lu, E.-G. Zhao, and S.-G. Zhou, *Phys. Rev. C* **85**, 011301(R) (2012).
 - [32] V. Prassa, T. Nikšić, and D. Vretenar, *Phys. rev. C* **88**, 044324 (2013).
 - [33] B.-N. Lu, J. Zhao, E.-G. Zhou, and S.-G. Zhou, *Phys. Rev. C* **89**, 014323 (2014).
 - [34] M. Bhuyan, S. K. Patra, and Raj K. Gupta, *J. Phys. G: Nucl. Part. Phys.* **42**, 015105 (2015).
 - [35] N. Schunck, and L. M. Robledo, *Rep. Prog. Phys.* **79**, 116301 (2016).
 - [36] M. Warda, J. L. Egido, L. M. Robledo, and K. Pomorski, *Phys. Rev. C* **66**, 014310 (2002).
 - [37] P. Madler, *Z. Phys. A* **321**, 343 (1985).
 - [38] M. S. Samanta, R. P. Anand, R. K. Choudhury, S. S. Kooper and D. M. Nadkarni, *Phys. Rev. C* **51**, 3127 (1995).
 - [39] L. Satpathy, S. K. Patra and R. K. Chouthury, *PRA-MANA J. Phys.* **70**, 87 (2008).
 - [40] A. Staszczak and Z. ojewski, *Nucl. Phys. A* **657**, 134 (1999).
 - [41] J. F. Berger, and K. Pomorski, *Phys. Rev. Lett.* **85**, 30 (2000). (2002).
 - [42] M. Warda, A. Staszczak and W. Nazarewicz, *Phys. Rev. C* **86**, 24601 (2012).
 - [43] W. Koepf and P. Ring, *Phys. Lett. B* **212**, 397 (1988).
 - [44] J. Fink, V. Blum, P.-G. Reinhard, J. A. Maruhn and W. Greiner, *Phys. Lett. B* **218**, 277 (1989).
 - [45] M. Leino, J. Äystö, T. Enqvist, P. Heikkinen, A. Jokinen, M. Nurmi, A. Ostrowski, W. H. Trzaska, J. Uusitalo, K. Eskola, P. Armbruster, and V. Ninov, *Nucl. Inst. and Meth. Phys. Res. B* **99**, 653 (1995).
 - [46] C. J. Gross, T. N. Ginter, D. Shapira, W. T. Milner, J. W. McConnell, A. N. James, J. W. Johnson, J. Mas, P. F. Mantica, R. L. Auble, J. J. Das, J. L. Blankenship, *et al.*, *Nucl. Inst. and Meth. Phys. Res. A* **450**, 12 (2000).
 - [47] Z. Sun, W. L. Zhan, Z. Y. Guo, G. Xiao, and J. X. Li, *Nucl. Inst. and Meth. Phys. Res. A* **503**, 496 (2003).
 - [48] M. Winkler, H. Geissel, H. Weick, B. Achenbach, K.-H. Behr, D. Boutin, A. Brnle, M. Gleim, W. Hüller, C. Karagiannis, A. Kelic, B. Kindler, *et al.*, *Nucl. Inst. and Meth. Phys. Res. B* **266**, 4183 (2008).
 - [49] H. Sakurai, *Nucl. Phys. A* **805**, 526c (2008).
 - [50] A. C. Mueller, and R. Anne, *Nucl. Inst. and Meth. Phys. Res. B* **56**, 559 (1991).

- [51] H. Geissel, P. Armbruster, K. H. Behr, A. Brünle, K. Burkard, M. Chen, H. Folger, B. Franczak, H. Keller, O. Klepper, B. Langenbeck, F. Nickel, *et al.*, Nucl. Inst. and Meth. Phys. Res. B **70**, 286 (1992).
- [52] A. M. Rodin, S. V. Stepantsov, D. D. Bogdanov, M. S. Golovkov, A. S. Fomichev, S. I. Sidorchuk, R. S. Slepnev, R. Wolski, G. M. Ter-Akopian, Y. T. Oganessian, A. A. Yukhimchuk, V. V. Perevozchikov, *et al.*, Nucl. Inst. and Meth. Phys. Res. B **204**, 114 (2003).
- [53] M. Thoennessen, Nucl. Phys. A **834**, 688c (2010).
- [54] S. Goriely, A. Bauswein, and H. T. Janka, Ast. Phys. J **738**, L32 (2011).
- [55] O. Korobkin, S. Rosswog, A. Arcones, and C. Winteler, MNRAS **426**, 1940 (2012).
- [56] O. Just O, A. Bauswein, R. A. Pulpillo, S. Goriely and H. T. Janka, MNRAS **448**, 541 (2015).
- [57] J. Boguta and A. R. Bodmer, Nucl. Phys. A **292**, 413 (1977).
- [58] B. D. Serot and J. D. Walecka, in *Advances in Nuclear Physics*, edited by J. W. Negele and Erich Vogt Plenum Press, New York, Vol. **16**, p. 1 (1986).
- [59] W. Pannert, P. Ring, and J. Boguta, Phys. Rev. Lett., **59**, 2420, (1986).
- [60] G. A. Lalazissis, S. Raman and P. Ring, Atm. Data. Nucl. Data. Table. **71**, 1 (1999).
- [61] S. K. Patra, M. Bhuyan, M. S. Mehta and Raj K. Gupta, Phys. Rev. C **80**, 034312 (2009).
- [62] P. -G. Reinhard, Rep. Prog. Phys. **52**, 439 (1989).
- [63] P. Ring, Prog. Part. Nucl. Phys. **37**, 193 (1996).
- [64] D. Vretenar, A. V. Afanasjev, G. A. Lalazissis, and P. Ring, Phys. Rep. **409**, 101 (2005).
- [65] J. Meng, H. Toki, S. G. Zhou, S. Q. Zhang, W. H. Long, and L. S. Geng, Prog. Part. Nucl. Phys. **57**, 470 (2006).
- [66] T. Nikšić, D. Vretenar, and P. Ring, Prog. Part. Nucl. Phys. **66**, 519 (2011).
- [67] D. Logoteta, I. Vidaña, C. Providência, A. Polls, and I. Bombaci, J. Phys. Conf. Ser. **342**, 012006 (2012).
- [68] Xian-Feng Zhao, and Huan-Yu Jia, Phys. Rev. C **85**, 065806 (2012).
- [69] G. A. Lalazissis, S. Karatzikos, R. Fossion, D. Pena Arteaga, A. V. Afanasjev, P. Ring, Phys. Lett. B **671**, 36 (2009).
- [70] P. Ring, Prog. Part. Nucl. Phys. **37**, 193 (1996).
- [71] B. A. Nikolaus, T. Hoch, and D. G. Madland, Phys. Rev. C **46**, 1757 (1992).
- [72] T. Burvenich, D. G. Madland, J. A. Maruhn, and P.-G. Reinhard, Phys. Rev. C **65**, 044308 (2002).
- [73] C. Fuchs, H. Lenske, and H. H. Wolter, Phys. Rev. C **52**, 3043 (1995).
- [74] T. Niksic, D. Vretenar, P. Finelli, and P. Ring, Phys. Rev. C **66**, 024306 (2002).
- [75] R. Brockmann and H. Toki, Phys. Rev. Lett. **68**, 3408 (1992).
- [76] Y. K. Gambhir, P. Ring, and A. Thimet, Ann. Phys. (N.Y.) **198**, 132 (1990).
- [77] G. A. Lalazissis, J. König, and P. Ring, Phys. Rev. C **55**, 540 (1997).
- [78] C. J. Horowitz and B. D. Serot, Nucl. Phys. A **368**, 503 (1981).
- [79] J. Boguta, Nucl. Phys. A **372**, 386 (1981).
- [80] C. E. Price, G. E. Walker, Phys. Rev. C **36**, 354 (1987).
- [81] S. Karatzikos, A. V. Afanasjev, G. A. Lalazissis, P. Ring, Phys. Lett. B **689**, 72 (2010).
- [82] J. Y. Zeng and T. S. Cheng, Nucl. Phys. A **405**, 1 (1983).
- [83] H. Molique and J. Dudek, Phys. Rev. C **56**, 1795 (1997).
- [84] T. V. N. Hao, P. Quentin, and L. Bonneau, Phys. Rev. C **86**, 064307 (2012).
- [85] G. A. Lalazissis, D. Vretenar, P. Ring, M. Stoitsov, and L. M. Robledo, Phys. Rev. C **60**, 014310 (1999).
- [86] J. Dobaczewski, H. Flocard, J. Treiner, Nucl. Phys. A **422**, 103 (1984).
- [87] D. G. Madland and J. R. Nix, Nucl. Phys. A **476**, 1 (1981).
- [88] P. Möller and J.R. Nix, At. Data and Nucl. Data Tables **39**, 213 (1988).
- [89] M. Bhuyan, B. V. Carlson, S. K. Patra, and S.-G. Zhou, Phys. Rev. C **97**, 034322 (2018).
- [90] P. Möller, J. R. Nix, W. D. Myers and W. J. Swiatecki, Atomic and Nucl. Data Tables **59**, 185 (1995).
- [91] P. Möller, J. R. Nix and K. -L. Kratz, Atomic and Nucl. Data Tables **66**, 131 (1997).
- [92] S. Goriely, F. Tondeur, J. M. Pearson, Atomic Data and Nucl. Data Tables **77**, 311 (2001).
- [93] M. Wang, G. Audi, A. H. Wapstra, F. G. Kondev, M. MacCormick, X. Xu, and B. Pfeier, Chinese Phys. C **36**, 1603 (2013).
- [94] I. Angeli, K. P. Marinova, Atomic Data and Nucl. Data Tables **99**, 69 (2013).
- [95] S. Raman, C. W. Nestor, JR., and P. Tikkanen, Atomic Data and Nucl. Data Tables **78**, 1 (2001).
- [96] R. Capote, M. Herman, P. Oblozinsky, P. Young, S. Goriely, T. Belgia, A. Ignatyuk, A. Koning, S. Hilaire, V. Plujko, M. Avrigeanu, O. Bersillon, M. Chadwick, T. Fukahori, Z. Ge, Y. Han, S. Kailas, J. Kopecky, V. Maslov, G. Reffo, M. Sin, E. Soukhovitskii, and P. Talou, *Special Issue on Nuclear Reaction Data*, Nucl. Data Sheets **110**, 3107 (2009).
- [97] H. Flocard, P. Quentin, and D. Vautherin, Phys. Lett. B **46**, 304 (1973).
- [98] W. Koepf and P. Ring, Phys. Lett. B **212**, 397 (1988).
- [99] S. Karatzikos, A. V. Afanasjev, G. A. Lalazissis, P. Ring, Phys. Lett. B **689**, 72 (2010).
- [100] N. Dubray, H. Goutte, and J.-P. Delaroche, Phys. Rev. C **77**, 014310 (2008).
- [101] L. Bonneau, Phys. Rev. C **74**, 014301 (2006).
- [102] D. M. Brink, *Int. School of Physics Enrico Fermi*, Course 36 (Berlin: Academic), (1996).